International Journal of Solids and Structures 58 (2015) 1–11

Contents lists available at ScienceDirect

International Journal of Solids and Structures

journal homepage: www.elsevier.com/locate/ijsolstr

Preventing interface damage by pre-conditioning polymer-coated steels via rolling

J. van Beeck [a,b,*], L.C.A. van Breemen [a], P.J.G. Schreurs [a], M.G.D. Geers [a]

[a] Department of Mechanical Engineering, Eindhoven University of Technology, De Rondom 70, 5612 AP Eindhoven, The Netherlands
[b] Materials innovation institute (M2i), Delft, The Netherlands

ARTICLE INFO

Article history:
Received 13 September 2014
Received in revised form 20 November 2014
Available online 24 December 2014

Keywords:
Damage prevention
Polymer-coated steel
Rolling
Interface roughening
Interface damage

ABSTRACT

A novel methodology is presented for pre-conditioning a polymer-coated steel used in food and beverage packaging. Mechanical rejuvenation of the coating via rolling is studied in order to prevent interface damage in subsequent forming operations. The simulations reveal that the thermodynamic state of the polymer coating after rolling depends on the rolling reduction. This dependency can be used to tailor the thermodynamic state of the coating prior to can production. A proof-of-principle simulation was performed to study the effects of rejuvenation on subsequent deformation processes. Deformation-induced interface roughening was studied for the initial and rejuvenated polymer coating. The predictions for a rejuvenated polymer coating indicate a significant decrease in interface damage.

The presented numerical framework allows for a detailed study of the effects of pre-conditioning on the interface integrity during subsequent forming operations. With properly identified material parameters, it becomes possible to tailor the polymer–steel material properties before and during production to minimize interface damage during production and storage of cans or canisters, e.g. for food and beverage packaging.

1. Introduction

Recent years show an increase in the use of metal-polymer laminates in the form of electrolytic chromium coated steel (ECCS) sheets coated with a polymer layer (see Fig. 1) for packaging of food and beverages. Producing cans and canisters using pre-coated steel leads to a significant reduction of the environmental impact of the production process compared to conventional production methods. Traditionally, a can is first made from blank steel sheet after which several lacquering steps are necessary to apply a protective coating on the inside and a decorative coating on the outside. The reduction in environmental impact results from a reduction in energy consumption and CO_2 emission with one third and a reduction in process water and resulting solid wastes to practically zero (Van der Aa et al., 2000).

However, the pre-coated steel is subjected to several forming stages during production, i.e. deep (re-) drawing (DRD) and wall-ironing (see Fig. 2). These processes induce large deformations at high strain rates, pressures and temperatures. It has been shown experimentally that the interface accumulates damage during production and sterilization. While this damage is often not visible after production, it may become apparent during the prolonged product shelf-life. The food packaging industry demands that the polymer coating fully adheres to the ECCS substrate, even after a relatively long shelf-life, since this triggers corrosion and compromises the quality of the canned content (Boelen et al., 2004; Van den Bosch et al., 2008).

An example of the typical intrinsic response of glassy polymers under uniaxial compression is shown in Fig. 3. First, the polymer shows a nearly linear elastic response (1) after which the response becomes non-linear visco-elastic (2). After the yield point (3) is reached, depending on the thermodynamic state of the polymer (i.e. its age), softening is observed (4), which is overtaken by strain hardening at high strains (5). A key characteristic of polymer glasses is the fact that the yield point depends on the strain rate applied (Van Breemen et al., 2011).

The yield point thus depends on the thermodynamic state. The thermodynamic state refers to the (non-) equilibrium state of a

Abbreviations: ECCS, electrolytic chromium coated steel; DRD, Deep-draw, deep-ReDraw; PET, Polyethylene terephthalate; EGP, Eindhoven Glassy Polymer model [10]; RD, rolling direction; FE-DIC, Finite Element based Digital Image Correlation.

* Corresponding author at: Department of Mechanical Engineering, Eindhoven University of Technology, De Rondom 70, 5612 AP Eindhoven, The Netherlands. Tel.: +31 40 247 5675.

E-mail address: J.v.Beeck@tue.nl (J. van Beeck).

http://dx.doi.org/10.1016/j.ijsolstr.2014.12.007
0020-7683/

glassy polymer, i.e. whether the polymer is close to or far away from its equilibrium state. When a polymer is cooled below its glass transition temperature (T_g), the mobility of the chains is decreased and the polymer moves away from equilibrium. However, the chain mobility is not zero and equilibrium will only be reached after an extended time, i.e. physical aging. The amount of softening seen in the mechanical response increases with physical aging. The process of moving the thermodynamic state of the polymer away from equilibrium, i.e. reverse aging, is called rejuvenation. Rejuvenation can be accomplished through a thermo-mechanical treatment (Klompen, 2005; Van Melick et al., 2003).

Recent results revealed the importance of the thermodynamic state of the polymer coating prior to deformation on the predicted interface damage (Van Beeck et al., 2015). A numerical–experimental study of the effect of deformation-induced interface roughening on the interface integrity of a polymer-coated steel indicated the existence of an optimum in the initial thermodynamic state of the PET (Polyethylene terephthalate) coating, i.e. the polymer age prior to deformation. A rejuvenated polymer shows (almost) no softening during mechanical deformation, while an aged polymer typically softens, see also Fig. 3. The simulations, which were performed using experimentally obtained full-field displacement fields of an evolving steel surface profile, predicted noticeably less interface damage for a rejuvenated coating compared to an aged coating. The changes in steel surface roughness trigger localization in the aged polymer coating, resulting in interface delamination. This localization behavior is significantly reduced for a rejuvenated coating, resulting in less damage.

After coating the steel substrate, the material is typically stored for extended periods of time. During this time, the coating ages continuously. Hence, rejuvenating the polymer coating towards the optimal initial thermodynamic state prior to production may decrease or even prevent the formation of interface damage.

It is well known that the thermodynamic state of a polymer can be tailored through a thermo-mechanical treatment (Van Melick et al., 2003). Thermal rejuvenation is accomplished by heating the polymer to a temperature above the glass transition temperature and then reducing the chain mobility via quenching. However, while a thermal treatment is relatively straightforward to apply in an industrial forming process, in the case of a polymer-coated steel it may lead to interface failure due to a mismatch in thermal expansion between the PET coating and steel substrate. Furthermore, the increased temperature required for rejuvenation may result in additional crystallization of the coating.

Another possibility is a mechanical rejuvenation procedure, e.g. rolling or ironing. The deformation imposed on the polymer-coated steel during such a procedure will induce stresses at the interface, i.e. normal and shear stresses, which may result in interface failure. However, a study by Van der Aa et al. (2000) showed that during wall-ironing of a polymer-coated steel the coating hardens due to the high pressure imposed on it. This hardening reduces the stress difference between the typically compliant polymer coating and the stiff steel substrate, since the post-yield response of the polymer depends on the hydrostatic pressure (Christiansen et al., 1971). However, wall-ironing induces large shear stresses in the material. Rolling may provide a more suitable mechanical rejuvenation method as the roll moves with the material to reduce the shear stresses. Similar to wall-ironing, a pressure is induced which is expected to reduce the stress mismatch further. Furthermore, the high pressure may delay or prevent crystallization of the PET coating (Zoller and Fakhreddine, 1994). Rolling the polymer-coated steel to tailor the thermodynamic state of the coating prior to production is thus an interesting pre-processing step to explore.

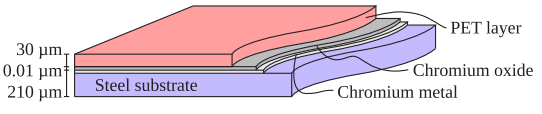

Fig. 1. Different material layers in a polymer coated ECC steel (after Van den Bosch et al. (2008)).

Several authors studied the effect of cold-rolling on the mechanical properties of polymers (Broutman and Patil, 1971; Matsuoka, 1998; Van Melick et al., 2003). Rolling of a coated material was investigated by Usov and Danilov (2007) by deriving the exact solution in case of an elastic coating and a rigid substrate material. A functionally graded elastic coating was recently studied by Guler and coworkers (Alinia et al., 2014; Guler et al., 2013). While these studies provide valuable insight into the mechanical behavior of a polymer during rolling, the behavior of a non-linear visco-elasto-plastic polymer coating on a steel substrate and the evolution of its thermodynamic state during rolling has not yet been investigated.

In this paper, the mechanical response of a metal-polymer bilayer material during rolling is investigated numerically using a non-linear visco-elasto-plastic material model for the PET coating. Furthermore, the change in the thermodynamic state is investigated as a means of pre-conditioning the material to prevent interface damage in subsequent deformation steps. Finally, the effect of the pre-conditioning on further deformation is studied in a proof-of-principle simulation of deformation-induced steel surface roughening.

The paper is organized as follows. The constitutive model and computational procedures for the rolling simulations are presented in Section 2. The simulation results are discussed in Section 3. The proof-of-principle simulations are presented in Section 4. The paper ends with a discussion in Section 5.

The following notations are adopted throughout the paper. A vector is denoted by $\vec{a}$ and a second-order tensor is denoted by $\mathbf{A}$. The inner product is defined as $\vec{a} \cdot \vec{b} = a_i b_i,\ i = 1,2,3$ and tensorial inner products as $\mathbf{A} \cdot \mathbf{B} = A_{ij}B_{jk}\vec{e}_i\vec{e}_k$ and $\mathbf{A} : \mathbf{B} = A_{ij}B_{ji}$. The transpose of a tensor is denoted by $\mathbf{A}^{\mathrm{T}}$ and the vector length is expressed as $||\vec{a}||$.

2. Constitutive and computational model

In this section, the material models for the polymer and steel are presented, along with their numerical implementation.

2.1. Polymer model

The studied coating consists of a PET layer with several additives to improve the PET–steel adhesion (Van den Bosch et al., 2008). PET is a glassy polymer and almost fully amorphous (crystallinity is approx. 8%). An example of the typical intrinsic behavior of amorphous glassy polymers under uniaxial compression is shown in Fig. 3. The intrinsic behavior of glassy polymers is thus complex and accurate modeling requires an advanced constitutive model.

In the past two decades, strong effort was put into accurately modeling the behavior of glassy polymers, e.g. the work of Boyce et al. (1988) and Govaert and co-workers (Van Breemen et al., 2011; Klompen et al., 2005). These models incorporate the non-linear visco-elastic behavior, as well as strain softening and hardening and the effects of temperature and time. Here, the so-called Eindhoven Glassy Polymer (EGP) model is adopted which adequately captures the complete intrinsic mechanical response of amorphous polymers (Van Breemen et al., 2011; Klompen et al., 2005). The EGP model is a multi-mode, multi-process constitutive model (Van Breemen et al., 2011). In the present work only one mode and one process is considered due to limited set of known PET

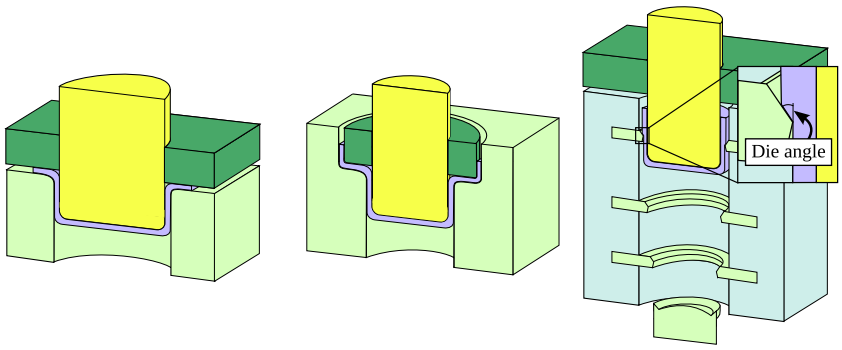

Fig. 2. Different production methods used to produce a can or canister (after CustomPartNet.com).

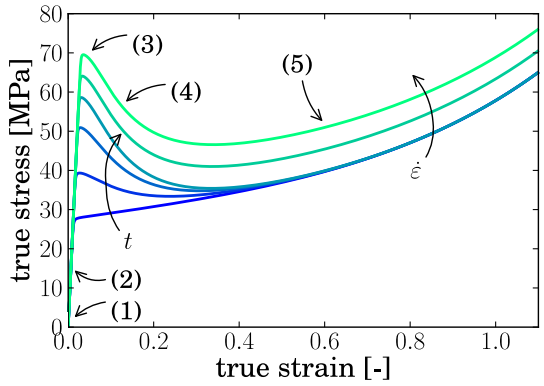

Fig. 3. Typical mechanical behavior of amorphous polymers; numbers indicate typical trends; (1) linear elastic; (2) non-linear visco-elastic; (3) yield point; (4) strain softening; and (5) strain hardening

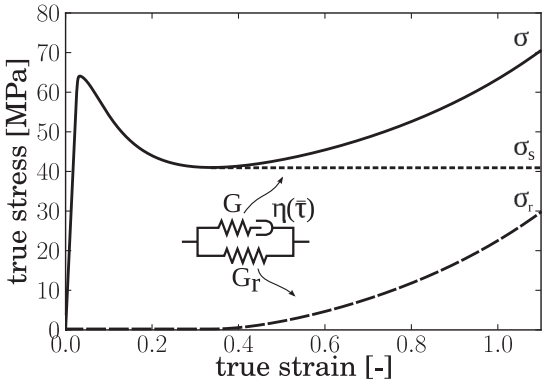

Fig. 4. Mechanical analogue of the SM-0SP EGP model (after Van Breemen et al. (2011)).

parameters, i.e. a single-mode, single-process approximation (SM–SP) is used. The mechanical analogue of the SM–SP EGP model is shown in Fig. 4. The essential equations of the SM–SP EGP model are detailed below.

In the EGP model the total stress is the addition of two contributions, i.e. the driving stress $\boldsymbol{\sigma}_s$ and the hardening stress $\boldsymbol{\sigma}_r$ (see also Fig. 4),

$$\boldsymbol{\sigma} = \boldsymbol{\sigma}_s + \boldsymbol{\sigma}_r. \tag{1}$$

The hardening stress originates from the rubber elastic contribution of the oriented entangled network and is described by a neo-Hookean relation,

$$\boldsymbol{\sigma}_r = G_r \tilde{\mathbf{B}}^d, \tag{2}$$

where G_r is the strain hardening modulus and $\tilde{\mathbf{B}}^d$ the deviatoric part of the isochoric left Cauchy-Green deformation (Finger) tensor. The driving stress incorporates the intermolecular interactions, i.e.

$$\boldsymbol{\sigma}_s = \boldsymbol{\sigma}_s^h + \boldsymbol{\sigma}_s^d = \kappa(J-1)\mathbf{I} + G\tilde{\mathbf{B}}_e^d, \tag{3}$$

where $\boldsymbol{\sigma}_s^h$ and $\boldsymbol{\sigma}_s^d$ are the hydrostatic and deviatoric stresses, respectively, κ is the bulk modulus, J is the volume change ratio, $\mathbf{I}$ is the second-order unity tensor, G is the shear modulus and $\tilde{\mathbf{B}}_e^d$ is the deviatoric part of the elastic isochoric Finger tensor. The quantities J and $\tilde{\mathbf{B}}_e^d$ evolve according to

$$\dot{J} = J\mathrm{tr}(\mathbf{D}), \tag{4}$$

$$\dot{\tilde{\mathbf{B}}}_e = (\tilde{\mathbf{L}} - \mathbf{D}_p)\cdot\tilde{\mathbf{B}}_e + \tilde{\mathbf{B}}_e\cdot(\tilde{\mathbf{L}}^{\mathrm{T}} - \mathbf{D}_p). \tag{5}$$

Here $\tilde{\mathbf{L}}$ is the isochoric velocity gradient tensor and $\mathbf{D}$ the deformation rate tensor. The plastic deformation rate tensor, $\mathbf{D}_p$ and $\boldsymbol{\sigma}_s^d$ are related by a non-Newtonian flow rule,

$$\mathbf{D}_p = \frac{\boldsymbol{\sigma}_s^d}{2\eta}, \tag{6}$$

with the viscosity

$$\eta = \eta_{0,ref}\frac{\bar{\tau}/\tau_0}{\sinh(\bar{\tau}/\tau_0)}\exp\left(\frac{\mu p}{\tau_0}\right)\exp(S), \tag{7}$$

where $\eta_{0,ref}$ is the zero-viscosity defined according to the reference state, τ_0 is the characteristic equivalent stress and μ is a pressure dependency parameter. The total equivalent stress, $\bar{\tau}$ and the pressure, p, are defined as

$$\bar{\tau} = \sqrt{\frac{1}{2}\boldsymbol{\sigma}_s^d : \boldsymbol{\sigma}_s^d}, \tag{8}$$

$$p = -\frac{1}{3}\mathrm{tr}(\boldsymbol{\sigma}). \tag{9}$$

The thermodynamic state parameter S contains the thermodynamic history dependence and is related to the equivalent plastic strain, $\bar{\varepsilon}_p$, i.e.

$$S(\bar{\varepsilon}_p) = S_a \cdot R(\bar{\varepsilon}_p). \tag{10}$$

Here S_a reflects the initial state of the polymer and $R(\bar{\varepsilon}_p)$ is a softening function, which incorporates the strain dependency of S. The softening function is described by a modified Carreau–Yasuda function (Klompen et al., 2005),

$$R(\bar{\varepsilon}_p) = \frac{\left(1 + \left(r_0\cdot\exp\left(\bar{\varepsilon}_p\right)\right)^{r_1}\right)^{(r_2-1)/r_1}}{\left(1 + r_0^{r_1}\right)^{(r_2-1)/r_1}}, \tag{11}$$

Table 1
Material properties of PET for the EGP model.

G_r [MPa]	κ [MPa]	G [MPa]	$\eta_{0,ref}$ [MPa s]	τ_0 [MPa]
4.7	1800	812	$3 \cdot 10^8$	1.262
μ [−]	S_a[−]	r_0[−]	r_1[−]	r_2[−]
$4.8 \cdot 10^{-2}$	13.3	0.98	20	−3.5

where r_0, r_1, r_2 are fitting parameters. R ranges between 0 (rejuvenated) and 1. In the current implementation the time dependence of S_a, i.e. physical aging is not included. Therefore, the yield stress does not increase with time and only the effect of mechanical rejuvenation is predicted with the present model. The equivalent plastic strain rate is defined as

$$\dot{\bar{\varepsilon}}_p = \frac{\bar{\tau}}{\eta}. \tag{12}$$

The PET material parameters used in this work are listed in Table 1 and the corresponding mechanical response during a uniaxial tensile test for an aged ($S_a = 13.3$ [−]) and rejuvenated ($S_a = 0$ [−]) PET layer is shown in Fig. 5(a). The parameters were taken from Poluektov et al. (2013) for a similar amorphous PET grade. The parameters are not fully exact for the PET coating considered here. However, the parameters predict realistic PET behavior.

2.2. Steel

Similar to the work of Van den Bosch et al. (2008), an isotropic elasto-plastic constitutive material model with a Von Mises yield criterion is used. Hardening is modeled using an isotropic power-law, i.e.

$$\sigma_y = H\left(\varepsilon_0 + \bar{\varepsilon}_p\right)^n, \tag{13}$$

where H, ε_0 and n are material parameters and $\bar{\varepsilon}_p$ is the effective plastic strain. The parameters are given by $H = 477$ [MPa], $\varepsilon_0 = 2 \cdot 10^{-3}$ [−] and $n = 0.1$ [−]. The Young's modulus is $E = 210$ [GPa] and the Poisson's ratio is $\nu = 0.3$ [MPa]. The mechanical response of the steel substrate is shown in Fig. 5(b).

2.3. Friction model

Friction between the roll and the PET coating is modeled using the Coulomb friction law, i.e.

$$||\vec{f}_t|| < \mu_f f_n, \quad \text{(stick)}, \tag{14}$$

$$\vec{f}_t = -\mu_f f_n \vec{t} \quad \text{(slip)}, \tag{15}$$

where $\vec{f}_t$ is the tangential friction force, and f_n is the normal force, μ_f is the friction coefficient and $\vec{t}$ is the tangential vector in the direction of the relative velocity $\vec{v}_r$ between the roll and the coating,

$$\vec{t} = \frac{\vec{v}_r}{||\vec{v}_r||}. \tag{16}$$

The transition between stick and slip is a step function, which is numerically inconvenient. Thus, $\vec{f}_t$ is approximated by an arctangent function, i.e.

$$\vec{f}_t = -\frac{2\mu_f f_n}{\pi} \arctan\left(\frac{||\vec{v}_r||}{\delta}\right)\vec{t}, \tag{17}$$

where the value of δ sets the value of the relative sliding velocity above which sliding occurs. In Van Breemen et al., 2011 it was found that $0.01 \cdot ||\vec{v}_r|| \leqslant \delta \leqslant 0.1 \cdot ||\vec{v}_r||$ gives realistic results. The friction coefficient is based on values commonly seen for PET and, unless otherwise stated, is set to $\mu_f = 0.2$ [−] (Samyn and Schoukens, 2008).

2.4. Computational model

The two-dimensional plane strain computational model for the rolling process is shown in Fig. 6. Obviously, the roll radius ($R = 35$ [mm]) is considerably larger than the thickness of the simulated material (steel: 105 [μm], PET: 15 [μm]). The roll is assumed to be infinitely stiff and is modeled as a rigid body. Symmetry is assumed along the bottom of the steel layer.

In the industrial forming process, the steel substrate is rolled to its desired thickness prior to applying the coating. The roll creates a smooth surface in the rolling direction (see also Fig. 13(a)). Here, the pre-conditioning rolling step is assumed to be performed in the rolling direction of the steel. It is therefore assumed that the initial surface profile of the steel, and hence the PET–steel interface, is flat.

Rolling is performed by moving the rotating roll over the polymer-coated steel at a fixed velocity $v = \omega \cdot R$, where ω is the rotational speed and R the radius of the roll. The right edge of the polymer-coated steel is fixed in the x-direction. Furthermore, considering that only part of a polymer-coated steel plate is modeled, the left edge is kept straight. This may result in edge effects near the right and left boundaries and thus only the response of the dashed central region (see Fig. 6) is analyzed. The dashed region is modeled as a separate body to study the PET–steel interface stress that develops during rolling. The interface stress is calculated from the force required to fix the dashed PET region to the steel substrate.

In the current simulations, the roll rotational speed is set to $\omega = 1.745 \cdot 10^{-3}\left[\text{rad} \cdot \text{s}^{-1}\right]$ to ensure that the applied strain rate during rolling stays within the experimental regime used to determine the EGP model parameters, i.e. the strain rate should not exceed $1 \cdot 10^{-2}$ [s^{-1}]. The commonly used industrial strain rate is higher, in the order of $1 \cdot 10^{3}$ [s^{-1}]. Simulating such high rolling

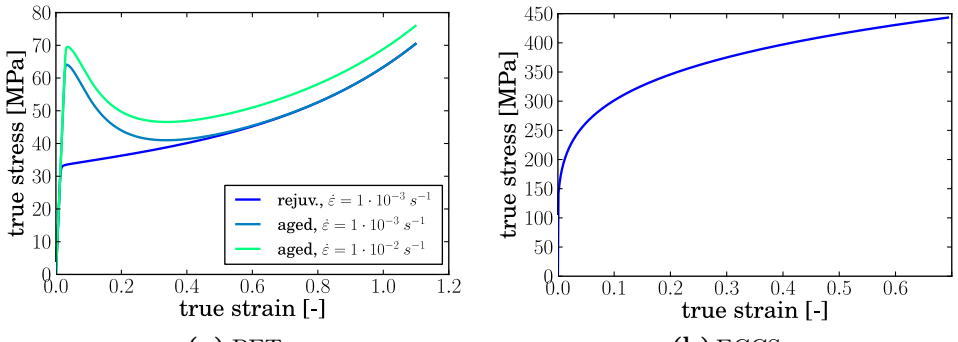

(a) PET (b) ECCS

Fig. 5. Mechanical response of the two modeled materials; note that $S_a = 0$ [−] for rejuvenated and $S_a = 13.3$ [−] for aged PET.

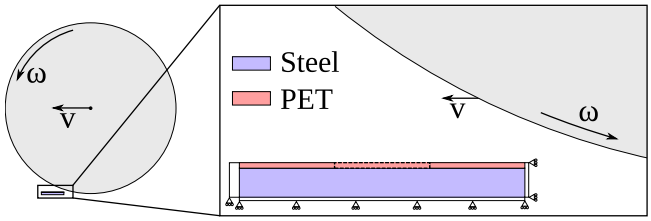

Fig. 6. Sketch of the simulated rolling process.

speeds requires dedicated experiments to quantify the PET response at higher strain rates. The increased strain rate may result in additional dynamical effects, i.e. the mismatch in strain rates allows for a qualitative prediction only.

As discussed in the introduction, the work of Van der Aa et al. (2000) revealed that the pressure imposed to the polymer coating during wall-ironing may reduce the interface stresses to prevent delamination. As rolling also imposes a pressure to the coating it can be assumed that the polymer–steel interface remains intact during rolling. Thus, for simplicity, the interface is not modeled explicitly, i.e. perfect adhesion is assumed. This assumption is investigated by analyzing the stress at the PET–steel interface.

3. Results

3.1. Evolution of the thermodynamic state

The evolution of the average value of the thermodynamic state parameter $\bar{S}$ as a function of time for a rolling reduction (i.e. the thickness reduction) of 10% and a friction coefficient of $\mu_f = 0.2$ [−] is shown in Fig. 7. $\bar{S}$ is the average thermodynamic state (S, see Eq. 10) within the dashed region in Fig. 6. Five stages can be identified, i.e. (1) initially the value remains constant as the roll has not yet entered the dashed region; (2) as soon as the roll starts to plastically deform the PET coating, the thermodynamic state parameter drops rapidly; (3) the parameter stabilizes shortly when the material passes underneath the roll; (4) a further drop in the parameter is noticed as the region of interest leaves the roll and starts to unload; and (5) finally, the value stabilizes at a value of approximately $S \approx 2$ [−].

The final average state parameter ($\bar{S}_{final}$, stage 5) as a function of the imposed rolling reduction is shown in Fig. 8. Clearly, the average thermodynamic state after rolling decreases from its initial value of $S_a = 13.3$ [−] with increasing rolling reduction. The dependence on the imposed reduction is non-linear with an initial steep decrease. Full rejuvenation ($S = 0$ [−]) is only reached for large

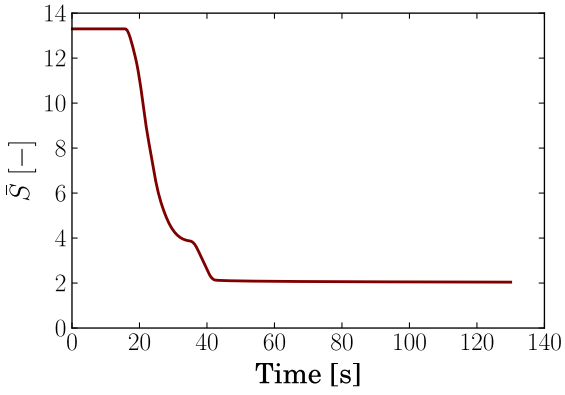

Fig. 7. Evolution of the average thermodynamic state parameter $\bar{S}$ as a function of time; rolling reduction 10%; friction coefficient $\mu_f = 0.2$ [−].

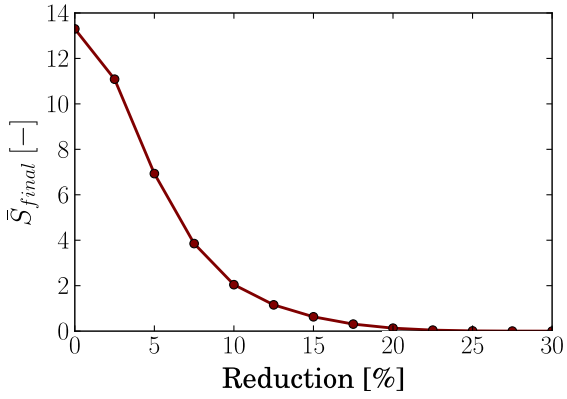

Fig. 8. Evolution of the final average thermodynamic state parameter $\bar{S}_{final}$ as a function of the rolling reduction; time 120 [s]; friction coefficient $\mu_f = 0.2$ [−].

rolling reductions. The numerical–experimental study presented in Van Beeck et al. (2015) showed that interface damage is minimized when the initial thermodynamic state of the coating prior to production is around $S \approx 2 - 2.5$ [−]. Rolling to a reduction of about 10% is thus desired to reach this optimum value.

3.2. Interface stress

The interface stress during rolling is shown in Fig. 9. The normal interface stress (Fig. 9(a)) is compressive during rolling and increases with increasing reduction. Compressive stresses applied to the interface typically do not result in interface damage. This is also commonly assumed in cohesive zone approaches where a negative opening results in interface strengthening (Van den Bosch et al., 2006). The tangential interface stress (Fig. 9(b)) shows an initial maximum, followed by a minimum. The extreme values of the stress clearly increase (in absolute sense) with increasing reduction. The interface must remain intact during rolling to withstand the tangential interface stress. Clearly, the higher the rolling reduction, the higher the interface stress. Whether the interface remains really intact during this process should be investigated experimentally.

3.2.1. Influence of friction

The influence of the friction coefficient on the interface stresses during rolling was investigated. The interface stress in normal and tangential direction for a friction coefficient varying between 0 and 0.3 is shown in Fig. 10. The compressive normal stress (Fig. 10(a)) increases with an increase in the friction coefficient. The tangential stress (Fig. 10(b)) shows a different trend. Three different extremes are visible in the stress during rolling, i.e. (1) a maximum when the material enters the roll (=entrance); (2) a minimum just after entering the roll (=under); and (3) another minimum as the material leaves the roll (=exit). The highest stress magnitude depends on the friction coefficient. Fig. 11 shows the magnitude of the tangential stress reached in the different stages during rolling. Clearly, the global maximum value is seen in different regions depending on the friction coefficient. For small values of the friction coefficient, the maximum tangential stress is reached when the material enters the roll. The friction reduces the interface stress in this regime as it guides the material under the roll and thus a decrease of this maximum is seen when the friction coefficient is increased. For high values of the friction coefficient the magnitude of the stresses under the roll increases. The location of the global maximum changes. The magnitude of the exit stress shows a less pronounced increase with increasing friction coefficient and typically is lower than the other two extreme values. Clearly, the

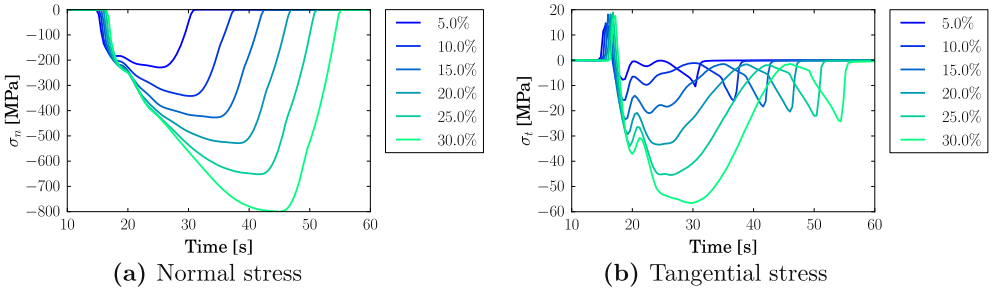

(a) Normal stress (b) Tangential stress

Fig. 9. (a) Normal and (b) tangential stresses acting on the interface during rolling for different rolling reductions; friction coefficient $\mu_f = 0.2$ [−].

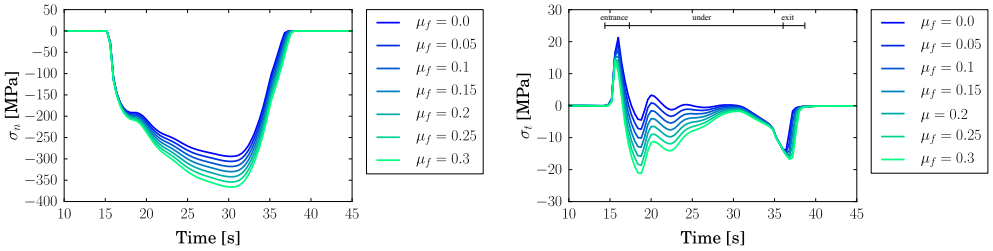

(a) Normal stress (b) Tangential stress

Fig. 10. (a) Normal and (b) tangential stresses acting on the interface during rolling for different friction coefficients; reduction is 10%.

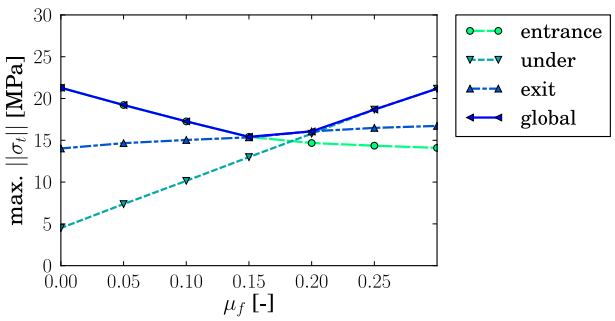

Fig. 11. Maximum magnitude of the tangential interface stress for different values of the friction coefficient and for different moments during rolling (see also Fig. 10(b)); reduction is 10%.

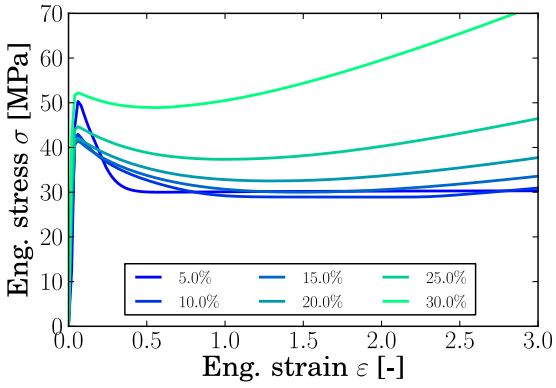

Fig. 12. Engineering stress–strain response of the PET coating after rolling the bilayer material to different rolling reductions; friction coefficient $\mu_f = 0.2$ [−].

magnitude of the interface stresses depends on the friction coefficient and an optimum in the coefficient exists which minimizes the maximum.

3.3. Influence on mechanical behavior

To characterize the effect of the rolling process on the mechanical behavior of the PET coating after rolling, the dashed central region of the PET coating (see Fig. 6) was subjected to a plane-strain tensile test after rolling. The resulting engineering stress–strain response for different rolling reductions and a friction coefficient of $\mu_f = 0.2$ [−] is shown in Fig. 12. The results predict softening for all simulated rolling reductions, i.e. a drop in the stress emerges after the yield point is reached. After rolling, small imperfections are present which trigger localization in the subsequent tensile test. Note that the softening in the response is dependent on the rolling reduction., i.e. a larger rolling reduction shows less softening in the tensile test.

These results are compared to the work of Broutman and Patil (1971), who studied the influence of rolling on the mechanical response of different polymers in a tensile test. These results apply to rolling of the polymer only and not for rolling of a polymer-coated steel, i.e. the results can be compared qualitatively only. The resulting dependency on the rolling reduction was also found by Broutman and Patil (1971), indicating that the predicted effect of rolling, at least qualitatively, compares well to experiments.

4. Proof-of-principle simulation

As mentioned in the introduction, the goal of pre-conditioning the polymer-coated steel via rolling is to delay or possibly prevent the initiation and growth of interface damage during subsequent forming operations. The previous section confirmed that rolling may provide a method to mechanically rejuvenate the coating to the desired optimal thermodynamic state. In order to assess the effect of the pre-conditioning, proof-of-principle simulations are performed next.

Recent experimental results revealed that deformation-induced roughening of the polymer–steel interface plays an important role in the initiation and growth of interface damage (Faber et al., 2013). During production, the polymer–steel interface experiences a significant change in roughness due to the deformation-induced

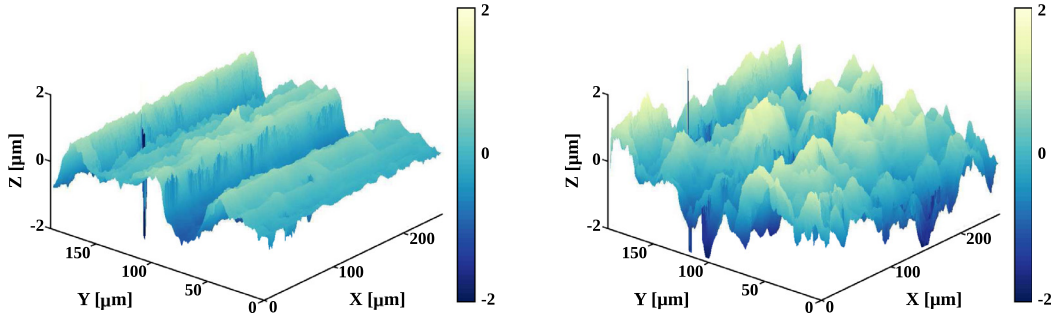

(a) Undeformed ECCS profile (b) ECCS profile just before fracture

Fig. 13. (a) Initial and (b) final surface profile of an ECC steel during a uniaxial tensile test, measured with a confocal optical profiler; *X*-direction is the tensile direction; colors indicate the local surface height in microns.

roughening of the steel substrate material. The polycrystalline steel roughens due to the differences in crystallographic orientation between grains and other plasticity related phenomena (Raabe et al., 2003). An example of this change in surface roughness for a packaging steel deformed in tension is shown in Fig. 13. The initial surface profile (Fig. 13(a)) is characterized by a rolling profile induced by the rolls (used to reduce the steel to its desired thickness). This profile is visible as grooves along the *x*-direction, i.e. in the rolling direction (RD). After performing a uniaxial tensile test in the *x*-direction to the steel, a change in roughness profile is measured, see Fig. 13(b). The comparison between the initial and final profile shows that the change in roughness occurs over a wide range of length scales, ranging from the scale of individual dislocations to the size of multiple grains. The resulting profile depends on the deformation conditions and the material properties (Raabe et al., 2003).

The numerical-experimental framework developed in Van Beeck et al. (2015) allows for a detailed study of the effect of a change in interface roughness on the interface integrity of these polymer-coated steels. This framework is here applied to illustrate the effect of the pre-conditioning on the interface integrity during subsequent deformation processes. Two simulations of deformation-induced interface roughening during a tensile test were performed, i.e. a simulation where the PET coating is aged ($S_a = 13.3$ [−]) and a simulation where the PET is rejuvenated to the optimal value ($S_a = 2.5$ [−]) prior to tensile testing.

For the simulations it is assumed that the internal stresses within the polymer layer after rolling are small. Furthermore, since it was assumed that the interface remains intact during pre-conditioning, the interface is initially intact. Finally, it is assumed that the surface roughness profile of the steel does not change during rolling. These assumptions limit the proof-of-principle simulation to a qualitative comparison of the effect of pre-conditioning only. For a quantitative prediction the full deformation history of the PET coating, interface and steel substrate must be taken into account. Quantitative predictions of the interface integrity and the deformation-induced steel surface roughening during rolling requires a steel constitutive model that accurately predicts the roughening process. However, quantitative models for predicting roughening in steels at multiple length scales are not yet available (Zhao et al., 2008).

4.1. Numerical–experimental framework

4.1.1. Experimental

A tensile test is performed along the rolling direction of TH340 packaging steel. TH340 is a continuously annealed, single reduced, DWI (draw-redraw-wall-ironing) quality Aluminum-killed low carbon ferritic ECCS sheet. The steel sheet is 210 [µm] thick. After each tensile strain increment of $\Delta\varepsilon = 0.25\%$, a confocal optical height measurement is taken. The initial and final surface profile are shown in Fig. 13. These confocal height profiles are used in a Finite Element based Digital Image Correlation method (FE-DIC) (Van Beeck et al., 2014) to extract the full-field displacement field that accompanies the change in surface roughness of the steel. The extracted displacement field along a line initially located on $y = 100$ [µm], shown in Fig. 14, is used in the proof-of-principle simulations.

The displacement field is applied in a two-dimensional plane strain simulation of a polymer-coated steel. As a result, the steel does not have to be modeled explicitly, since the measured experimental displacements are directly applied to the interface. A sketch of the computational model is shown in Fig. 15. The PET coating is modeled using the EGP model with the parameters listed in Table 1.

4.1.2. Interface model

The interface between the PET and ECCS is modeled using Cohesive Zone elements. The mixed-mode traction–separation law developed by Van den Bosch et al. (2006) is used to describe the PET–steel interfacial decohesion,

$$T_n(\Delta_n, \Delta_t) = \frac{\phi_n \Delta_n}{\delta_n^2} \exp\left(-\frac{\Delta_n}{\delta_n}\right) \exp\left(-\frac{\Delta_t^2}{\delta_t^2}\right), \tag{18}$$

$$T_t(\Delta_n, \Delta_t) = 2\frac{\phi_t \Delta_t}{\delta_t^2}\left(1 + \frac{\Delta_n}{\delta_n}\right) \exp\left(-\frac{\Delta_n}{\delta_n}\right) \exp\left(-\frac{\Delta_t^2}{\delta_t^2}\right), \tag{19}$$

where n and t are the normal and tangential directions, respectively, Δ is the cohesive zone opening, ϕ is the work of separation and δ is the characteristic opening length. The typical traction–separation response is shown in Fig. 16.

An integrity parameter ξ is used to quantify the fraction of the work of separation that is not yet dissipated in the cohesive zone element (Van Beeck et al., 2015),

$$\xi = 1 - \frac{\Omega}{\phi}, \quad \xi \in [0, 1], \tag{20}$$

where Ω is the consumed work of separation in the cohesive zone.

To determine the parameters of the cohesive law, dedicated experiments are needed. It is known from literature that different parameters may result from different experiments (Vossen et al., 2014). An example of two experiments that result in a different work of separation (ϕ) are the measurements of Fedorov et al. (2007) and Van den Bosch et al. (2008). The differences are explained by the distinct energy dissipated within the process zone, i.e. in the bulk material near the interface. For the proof-of-

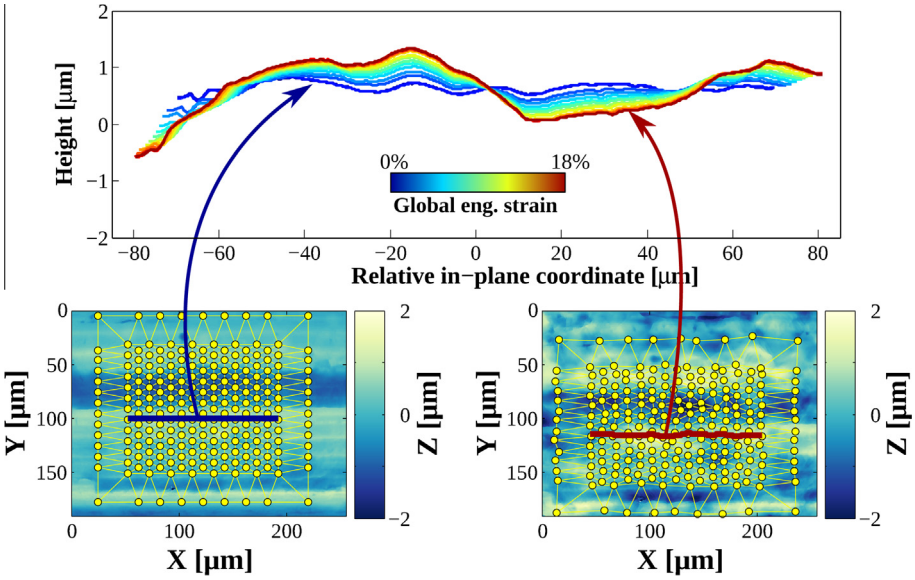

Fig. 14. Evolution of a line profile initially located at $y = 100$ [µm].

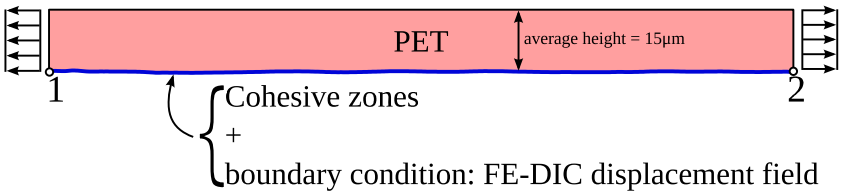

Fig. 15. Sketch of the computational framework (after Van Beeck et al. (2015)).

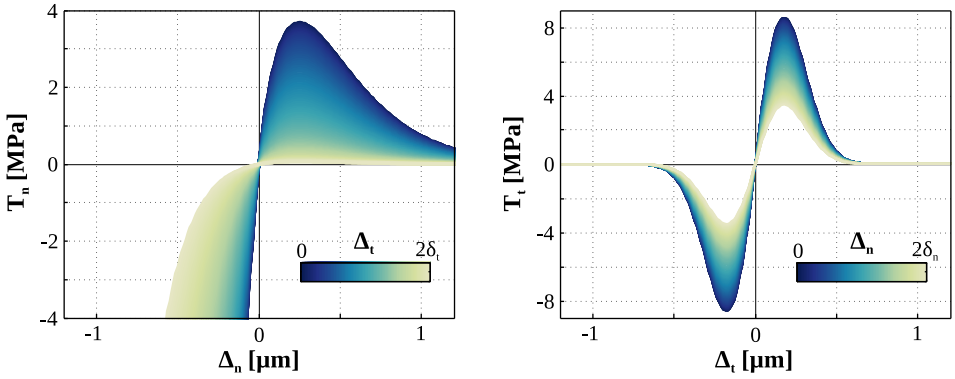

Fig. 16. The coupled exponential traction–separation law of Van den Bosch et al. (2006), using the parameters of Table 2.

principle simulations, parameters are required that are characteristic for small-scale de-bonding (Faber et al., 2013). The work of separation determined by Fedorov et al. (2007) is used here. As the cohesive law used is different, the δ_n and δ_t parameters are estimated based on the results in Fedorov et al. (2007). The resulting parameters used are listed in Table 2. Note that $\phi_n = \phi_t = \phi$ and $\delta_n = \delta_t = \delta$.

4.2. Results

The equivalent Von Mises stress and the equivalent plastic strain in the aged PET coating ($S_a = 13.3$ [−]) at a global tensile strain of $\varepsilon = 6\%$ and $\varepsilon = 11.5\%$ is shown in Figs. 17 and 18, respectively. The strains show pronounced localization with delamination at the interface as a result. The high stress in the localization band triggers interface damage (see Fig. 17). This damage grows as the deformation increases, see Fig. 18. The simulation of the mechanically rejuvenated coating at a global tensile strain of $\varepsilon = 11.5\%$ is shown in Fig. 19. A clear difference in predicted inter-

Table 2
Cohesive zone constants used in the proof-of-principle simulations.

ϕ_n [J m^{-2}]	ϕ_t [J m^{-2}]	δ_n [µm]	δ_t [µm]
2.5	2.5	0.25	0.25

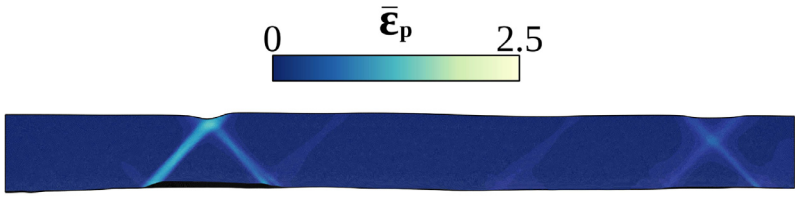

(a) Equivalent Von Mises stress

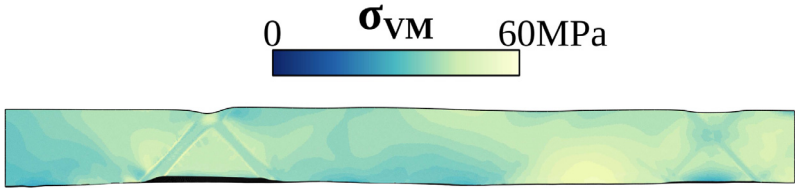

(b) Equivalent plastic strain

Fig. 17. Predicted equivalent Von Mises stress (a) and equivalent plastic strain (b) in the aged polymer coating along the line initially located at $y = 100$ [μm] at a globally applied tensile strain of $\varepsilon = 6\%$; the failed interface elements are colored black.

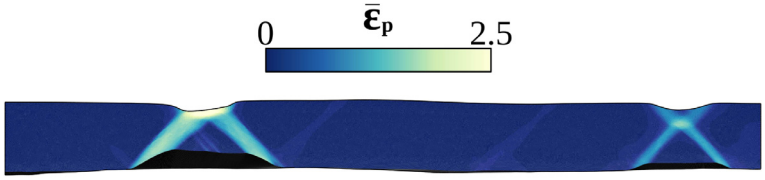

(a) Equivalent Von Mises stress

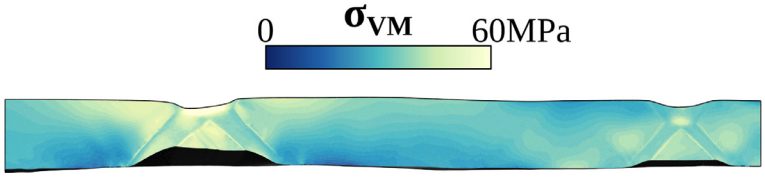

(b) Equivalent plastic strain

Fig. 18. Predicted equivalent Von Mises stress (a) and equivalent plastic strain (b) in the aged polymer coating along the line initially located at $y = 100$ [μm] at a globally applied tensile strain of $\varepsilon = 11.5\%$; the failed interface elements are colored black.

face damage is visible compared to the damage depicted in Fig. 18. Rejuvenation removes or reduces the softening branch from the intrinsic PET response (see also Fig. 5(a)). This softening triggers the localization events in the aged PET coating. The localization in case of the rejuvenated PET coating is clearly less pronounced.

The interface integrity over the line profile at a global tensile strain of $\varepsilon = 11.5\%$ is shown in Fig. 20. A large drop in the interface integrity is visible for the aged coating, see Fig. 20(a). However,the simulation with the rejuvenated PET coating shows significantly less reduction in integrity, indicating that less interface damage occurs, see Fig. 20(b).

5. Discussion

The rolling simulations of a polymer-coated steel enabled a detailed study of the evolution of the thermodynamic state of the coating as a function of the rolling reduction and other parameters.

Dedicated experiments are required to assess the validity of assumptions used in the rolling simulations, e.g. the assumed perfect adhesion. An indication of the validity of this assumption is provided by the interface stress that develops during rolling (see Fig. 9). Clearly, the stresses depend on the reduction. The normal interface stress (σ_n) is always in compression due to the rolling process, which typically does not damage the interface. However, the tangential interface stress also increases with increasing reduction, which may lead to interface damage. Thus, to reduce the interface stress, the reduction has to be minimized. However, a minimum reduction is required to rejuvenate the PET coating to the desired thermodynamic state and thus cannot be chosen arbitrarily. Research by Van der Aa et al. (2000) showed that during wall-ironing the imposed pressure hardens the PET coating. It was found that decreasing the die angle during wall-ironing (see Fig. 2(c)) resulted in a more distributed compressive stress. Although the deformation conditions during wall-ironing are different from those in rolling, it is expected that also here the effect of pressure is paramount. The hardening of the PET coating decreases the stress mismatch between the coating and the steel substrate. This may lower the interface stress during rolling. Thus,

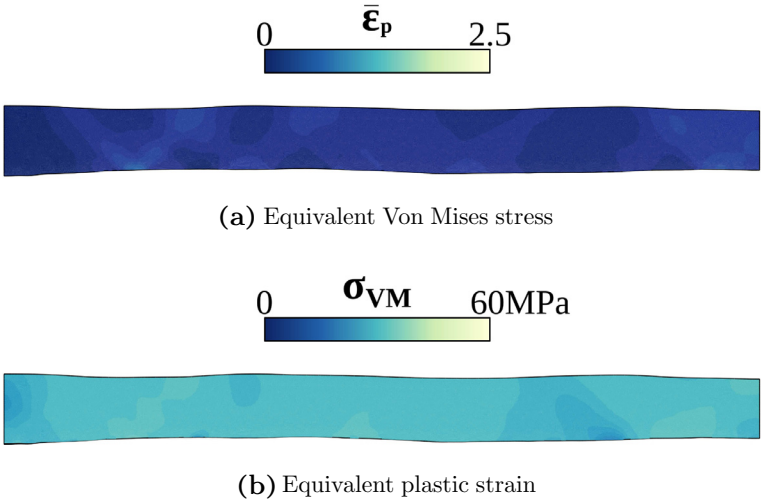

(a) Equivalent Von Mises stress

(b) Equivalent plastic strain

Fig. 19. Predicted equivalent Von Mises stress (a) and equivalent plastic strain (b) in the rejuvenated polymer coating along the line initially located at $y = 100$ [μm] at a globally applied tensile strain of $\varepsilon = 11.5\%$; the failed interface elements are colored black.

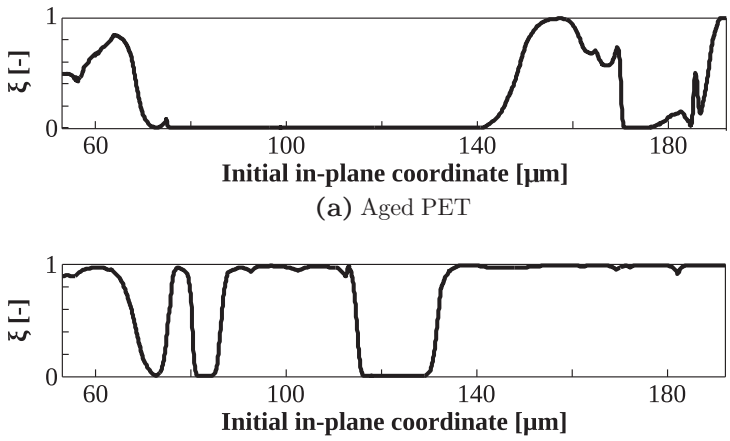

(a) Aged PET

(b) Rejuvenated PET

Fig. 20. Interface integrity profile at $\varepsilon = 11.5\%$ for the aged (a) and rejuvenated (b) PET over the line initially located at $y = 100$ [μm].

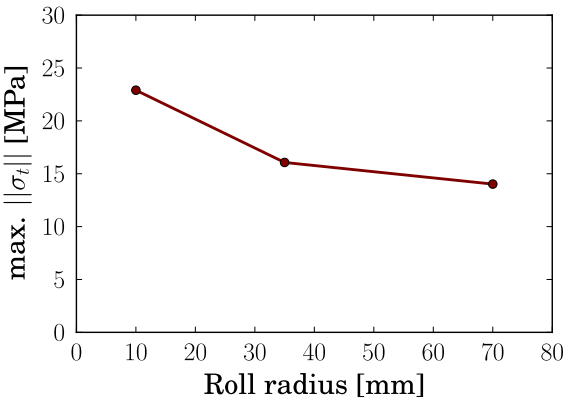

Fig. 21. Maximum magnitude of the tangential interface stress as a function of the roll radius; reduction 10%; friction coefficient $\mu_f = 0.2$ [–].

changing the roll radius may decrease the interface stress further. Fig. 21 shows the effect of changing the roll radius on the magnitude of the tangential interface stress during rolling, confirming the expected influence on the interface stress. The roll must be sufficiently large to prevent interface failure. Furthermore, the study on the effect of the friction coefficient revealed an optimum value which reduces the maximum magnitude of the tangential interface stress to a minimum. Whether the friction coefficient can be optimized has to be investigated experimentally.

The proof-of-principle simulations currently only include the change in thermodynamic state of the coating. The simulations may be extended to a coupled analysis where the polymer-coated steel is first rolled, after which a subsequent deformation process is applied. It is expected that a coupled study may reveal a different optimum for the thermodynamic state, as full rejuvenation of the coating requires a large reduction in thickness (see also Fig. 8), which increases the stresses at the interface. However, the conclusion that the rejuvenated material shows less interface damage is expected to persist.

6. Conclusion

A novel methodology was presented for pre-conditioning a polymer-coated steel used in food and beverage packaging. Previous research showed that pre-conditioning the thermodynamic state of the polymer coating prior to production may significantly reduce damage in the interface during production. In this paper,

the prior mechanical rejuvenation of the coating via rolling was explored. Numerical simulations of rolling were performed on a polymer-coated steel and the evolution of the thermodynamic state of the coating was studied. The simulations showed that changing the rolling reduction allows for optimization of the thermodynamic state. Furthermore, proof-of-principle simulations were performed using a previously developed numerical-experimental framework to study the effect of the rejuvenation on subsequent deformation. Deformation-induced steel surface roughening was simulated and predicted interface damage was compared to a simulation without pre-conditioning. The comparison revealed a significant decrease in predicted interface damage after rejuvenating the polymer coating.

The simulations provide valuable insight into the influence of rejuvenating a polymer coating and can be used to optimize the industrial process to reduce or even prevent interface delamination.

Acknowledgments

This research was carried out under the project number M63.2.09343a in the framework of the Research Program of the Materials innovation institute (M2i) (www.m2i.nl). Furthermore, Rens Verhees and Dion Visser are gratefully acknowledged for their contribution to the numerical framework.

References

Van der Aa, H.C.E., Van der Aa, M.A.H., Schreurs, P.J.G., Baaijens, F.P.T., Van Veenen, W.J., 2000. An experimental and numerical study of the wall ironing process of polymer coated sheet metal. Mech. Mater. 32, 423–443.

Alinia, Y., Guler, M.A., Adibnazari, S., 2014. On the contact mechanics of a rolling cylinder on a graded coating. Part 1: analytical formulation. Mech. Mater. 68, 207–216.

Van Beeck, J., Neggers, J., Schreurs, P.J.G., Hoefnagels, J.P.M., Geers, M.G.D., 2014. Quantification of three-dimensional surface deformation using global digital image correlation. Exp. Mech. 54, 557–570.

Van Beeck, J., Schreurs, P.J.G., Geers, M.G.D., 2015. Numerical–experimental assessment of roughness-induced metal-polymer interface failure. Mech. Mater. 8, 234–245.

Boelen, B., Den Hartog, H., Van der Weijde, H., 2004. Product performance of polymer coated packaging steel, study of the mechanism of defect growth in cans. Prog. Org. Coat. 50, 40–46.

Van den Bosch, M.J., Schreurs, P.J.G., Geers, M.G.D., 2006. An improved description of the exponential Xu and Needleman cohesive zone law for mixed-mode decohesion. Eng. Fract. Mech. 73, 1220–1234.

Van den Bosch, M.J., Schreurs, P.J.G., Geers, M.G.D., Van Maris, M.P.F.H.L., 2008. Interfacial characterization of pre-strained polymer coated steel by a numerical–experimental approach. Mech. Mater. 40, 302–317.

Van den Bosch, M.J., Schreurs, P.J.G., Geers, M.G.D., 2008. Identification and characterization of delamination in polymer coated metal sheet. J. Mech. Phys. Solids 56, 3259–3276.

Boyce, M.C., Parks, D.M., Argon, A.S., 1988. Large inelastic deformation of glassy polymers. Part I: rate dependent constitutive model. Mech. Mater. 7, 15–33.

Van Breemen, L.C.A., Klompen, E.T.J., Govaert, L.E., Meijer, H.E.H., 2011. Extending the EGP constitutive model for polymer glasses to multiple relaxation times. J. Mech. Phys. Solids 59, 2191–2207.

Broutman, L.J., Patil, R.S., 1971. Cold rolling of polymers. 1 influence of rolling on properties of amorphous polymers. Polym. Eng. Sci. 11, 165–173.

Christiansen, A.W., Baer, E., Radcliffe, S.V., 1971. The mechanical behaviour of polymers under high pressure. Philos. Mag. 24, 451–467.

Faber, E.T., Vellinga, W.P., De Hosson, J.T.M., 2013. Local delamination on heavily deformed polymer–metal interfaces: evidence from microscopy. J. Mater. Sci. 49, 691–700.

Fedorov, A.V., Van Tijum, R., Vellinga, W.P., De Hosson, J.T.M., 2007. Degradation and recovery of adhesion properties of deformed metal–polymer interfaces studied by laser induced delamination. Prog. Org. Coat. 58, 180–186.

Guler, M.A., Alinia, Y., Adibnazari, S., 2013. On the contact mechanics of a rolling cylinder on a graded coating. Part 2: numerical results. Mech. Mater. 66, 134–159.

Klompen, E.T.J., Engels, T.A.P., Van Breemen, L.C.A., Schreurs, P.J.G., Govaert, L.E., Meijer, H.E.H., 2005. Quantitative prediction of long-term failure of polycarbonate. Macromolecules 38, 7009–7017.

Klompen, E.T.J., 2005. Mechanical properties of solid polymers: constitutive modelling of long and short term behaviour (Ph.D. thesis). Eindhoven University of Technology (Chapter 1).

Matsuoka, S., 1998. Effects of cold-rolling on the cold forging of solid polymer. J. Mater. Process. Technol. 84, 175–180.

Van Melick, H.G.H., Govaert, L.E., Meijer, H.E.H., 2003. Localisation phenomena in glassy polymers: influence of thermal and mechanical history. Polymer 44, 3579–3591.

Poluektov, M., Van Dommelen, J.A.W., Govaert, L.E., Yakimets, I., Geers, M.G.D., 2013. Micromechanical modelling of short-term and long-term large-strain behaviour of polyethylene terephthalate. Model. Simul. Mater. Sci. Eng. 21, 085015.

Raabe, D., Sachtleber, M., Weiland, H., Scheele, G., Zhao, Z., 2003. Grain-scale micromechanics of polycrystal surfaces during plastic straining. Acta Mater. 51, 1539–1560.

Samyn, P., Schoukens, G., 2008. Experimental extrapolation model for friction and wear of polymers on different testing scales. Int. J. Mech. Sci. 50, 1390–1403.

Usov, P.P., Danilov, V.D., 2007. Contact problem for elastic layer and rigid cylinder with friction forces. J. Friction Wear 28, 225–238.

Vossen, B.G., Schreurs, P.J.G., Van der Sluis, O., Geers, M.G.D., 2014. Multi-scale modelling of delamination through fibrillation. J. Mech. Phys. Solids 66, 117–132.

Zhao, Z., Ramesh, M., Raabe, D., Cuitiño, A.M., Radovitzky, R., 2008. Investigation of three-dimensional aspects of grain-scale plastic surface deformation of an aluminum oligocrystal. Int. J. Plast. 24, 2278–2297.

Zoller, P., Fakhreddine, Y.A., 1994. Pressure–volume–temperature studies of semi-crystalline polymers. Thermochim. Acta 238, 397–415.